

LETTERS

Directly Resolved Core-Corona Structure of Block Copolymer Micelles by Cryo-Transmission Electron Microscopy

Yi Zheng, You-Yeon Won, Frank S. Bates, H. Ted Davis, and L. E. Scriven*

Department of Chemical Engineering & Materials Science and Center for Interfacial Engineering, University of Minnesota, Minneapolis, Minnesota 55455

Y. Talmon

Department of Chemical Engineering, Technion-Israel Institute of Technology, Haifa 32000, Israel

Received: July 12, 1999; In Final Form: September 20, 1999

Core-corona structures of poly(ethyleneoxide)/polybutadiene (PEO/PB) block copolymer micelles are directly resolved for the first time by examining rapidly vitrified samples by transmission electron microscopy at liquid nitrogen temperature (Cryo-TEM). Spherical micelles form at higher PEO/PB block volume ratio; cylindrical form at lower block volume ratio. Images of both shapes of micelles show a dense core and a diffuse corona. The core and corona sizes agree well with theoretical prediction from the "star" model of polymer micelles.

Introduction

Diblock copolymers can be viewed as the macromolecular counterparts of ordinary surfactants. An A-B block copolymer in a solvent that dissolves A but not B forms aggregates that are analogous to surfactant micelles. The micelles are generally pictured as spherical objects with two concentric regions: a core of blocks insoluble in the solvent, and a corona of soluble blocks swollen by the solvent. The corona amounts to a "polymer brush",^{2,3} i.e., polymer chains anchored to an interface by their ends. So constrained, the chains behave differently from unconstrained chains that adopt random-walk configurations.

Since the pioneering models of polymer brushes on flat surfaces were advanced,^{4,5} a major focus of theoretical analysis has been the brushes on highly curved interfaces. Several approaches have been used to model these systems, including molecular dynamics simulations,⁶ self-consistent-field (SCF) theories,⁷⁻¹⁰ and scaling theories.^{11,12} The polymer segment

density profile is the central issue of all the theoretical analyses. The SCF theories, which include lattice¹³ and continuum approaches,⁷ predict a parabolic density profile of brushes on planar interfaces⁷ and a concave profile of those on high-curvature interfaces.^{8,9} Block copolymer micellar systems, with their unique core-corona structure and spherical or cylindrical shapes, are good model systems of brushes on curved interfaces. Two limiting structures of the polymeric micelles are "crew-cut" micelles, which have short corona chains on a large core, and "long-hair" micelles, which have an extended corona and a small core. The mean density model¹⁴ has been used to approximate the crew-cut micelles; this model rests on the simplification that polymer concentration is constant in both the core region and the corona region⁵ (Figure 1a). The "star model" of long-hair micelles,¹ which is based on the scaling model of star polymers,¹² shows a power law decay in segment density (Figure 1b); in this model, the extended corona region is apportioned into shells made up of spherical blobs whose size in successive shells increases geometrically.

* Corresponding author.

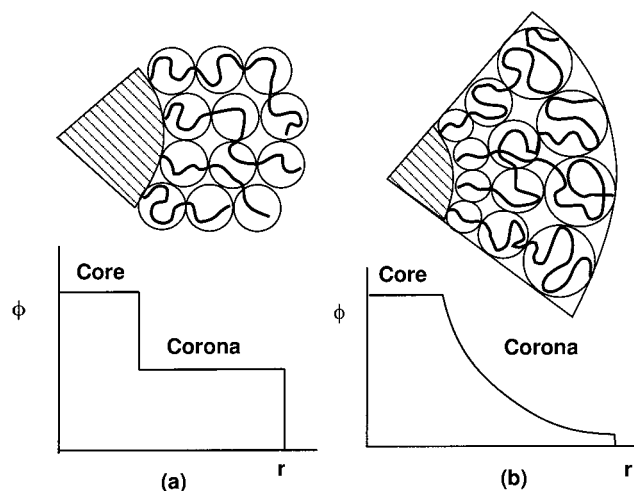


Figure 1. Models of the A–B diblock copolymer micelle in a selective solvent which dissolves A but not B. Schematic cross-sections and plots of monomer volume fraction f vs distance from the micelle center “ r ”. The core region consists of a melt of B blocks; the corona region consists of stretched A chains swollen by the solvent. (A) The mean density model; (B) the star model. The extended corona region is apportioned into shells of blobs. The blob size in successive shells expands geometrically. Within a blob, the polymer resembles a self-avoiding walk.

TABLE 1: Physical Properties of PEO–PB Block Copolymers^a

	$f(\text{PEO}) =$ $M_{\text{PEO}}/M_{\text{total}}$	M_{PEO}	M_{PB}	M_{total}	polydispersity
EO ₁₂₆ –B ₄₅	0.70	5670	2430	8100	1.09
EO ₁₆₆ –B ₁₀₄	0.57	7476	5633	13100	1.09
EO ₅₆ –B ₄₅	0.51	2499	2401	4900	1.15

^a Here the nomenclature adopted is similar to that used with nonionic surfactants, EO_{*i*}–B_{*j*}, where *i* and *j* denote the number of repeat units.

The corona (polymer brush) microstructure remains largely unclear, despite the experimental attempts by neutron scattering^{15,16} and reflectometry,^{17,18} static and dynamic light scattering,^{19–21} X-ray scattering,²² ellipsometry,²³ AFM,²³ and NMR.²⁴ To infer microstructure from these techniques is indirect in the sense that one has to assume a structural model, calculate the expected experimental outcome, and compare this with the actual experimental result. Moreover, the measured quantity is averaged over a certain sample volume, making it hard to distinguish between core and corona of individual micelles. Transmission electron microscopy (TEM) is a good local structural probe and the only technique that allows real-space imaging of three-dimensional objects at high resolution; and only rapid vitrification cryogenic TEM (Cryo-TEM) enables model-independent direct imaging of microstructures in liquid solution originally at ambient temperatures.²⁵ The corona of block copolymer micelles has, however, been believed to be invisible to Cryo-TEM because of its low electron density and thus low contrast.²⁶ Here we report the first direct imaging of the core-corona structure of polymeric micelles.

Poly(ethyleneoxide-*b*-butadiene) (PEO–PB) diblock copolymers with various PB and PEO block lengths (Table 1) were synthesized by anionic polymerization and characterized as described elsewhere.²⁷ Aqueous solutions of each polymer (1 wt %) were prepared with water from a Millipore UV coupled with a Millipore Q water purification system. Sample solutions were equilibrated for 1 month, after which they all appeared bluish, but no precipitation or floc could be detected by the naked eye. A 10–200 nm thick liquid film of sample solution

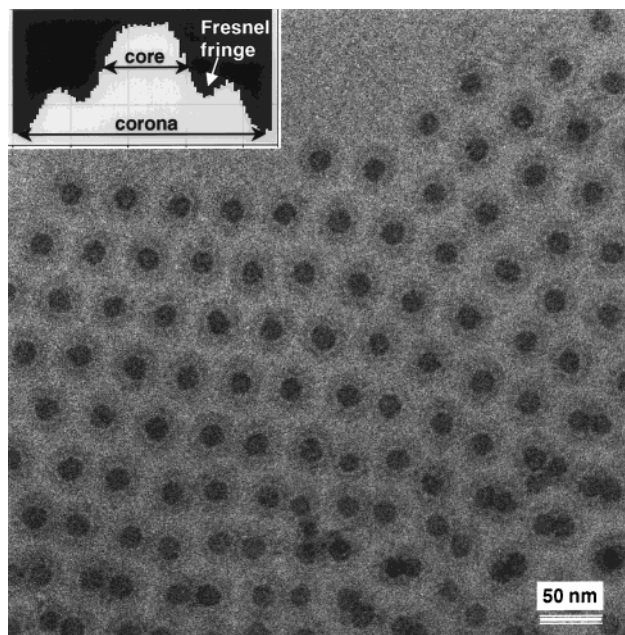


Figure 2. A Cryo-TEM micrograph of 1 wt % aqueous EO₁₂₆–B₄₅ diblock copolymer solution. A dark core consisting of PB blocks and a corona of PEO blocks is evident. The segment density profile of one micelle is shown in the inset. The best phase contrast was achieved with nominal objective lens under-focus of 0.7 μm . The spherical micelles are ordered in a fairly regular hexagonal array, presumably in response to the thickness gradient (from 10 to 20 nm to 200–300 nm) of the biconcave film. Fresnel fringe is indicated by the arrow in the micrograph.

was prepared, at 25 °C in air saturated with water vapor, on a perforated carbon film (holes ranging from 1 to 10 μm in diameter) supported on a 200-mesh TEM copper grid. The specimen was then vitrified by plunging it into liquid ethane at its freezing point. The vitrified samples were mounted on an Oxford CT-3500 cryo-holder and transferred into a Philips CM120 TEM with an Oxford work station. Specimens were imaged at nominal under defocus of 0.7 to 4 μm which provided maximum phase contrast. Specimen temperature was maintained below –170 °C during sample observation. All images were recorded with a Gatan 791 MultiScan digital camera and processed with DigitalMicrograph 3.1. Digital imaging leads to a cleaner vacuum because wet film is not introduced into the microscope, and so no contamination from this source condenses on the specimen. High magnification images were recorded with as low electron doses as practicable (on the order of 104 electrons/nm²) in order to minimize electron-beam radiation damage to the specimen.

A representative micrograph of spherical micelles formed by EO₁₂₆–B₄₅ is shown in Figure 2. The micelles are embedded in a free span of film of vitreous ice thin enough to be sufficiently “transparent” to the electron beam. A dark core and surrounding halo are evident and are confirmed by the optical density profile. Whereas the dark core corresponds to a PB domain, the halo must correspond to extended PEO chains that scatter electrons more strongly than water ice but less so than densely packed PB chains. Judged by its width and optical density, the halo cannot be a Fresnel fringe (as indicated by the arrow in the micrograph). This was borne out by thru-focus serial imaging: as the defocus is varied from under-focus to on-focus, a Fresnel fringe fades and finally disappears—but the halo remains (not shown). The density profile of one micelle is shown in the inset; it was converted from gray scale optical density of the image by DigitalMicrograph 3.1 on the assump-

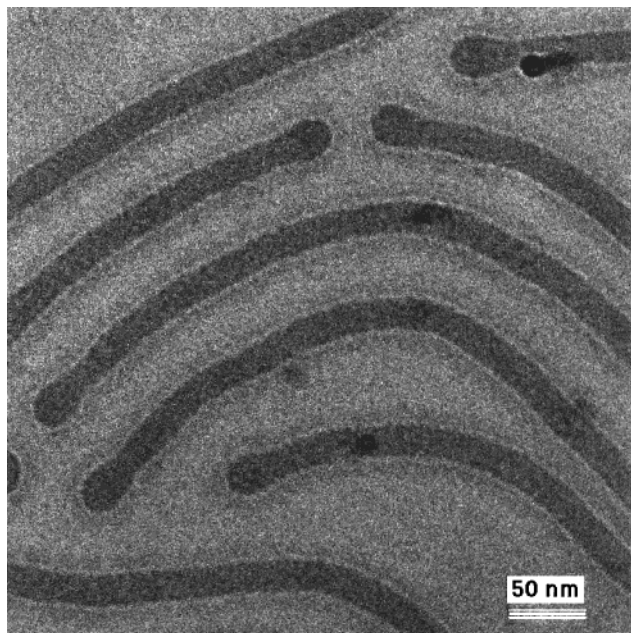


Figure 3. Cylindrical micelles formed in 1 wt % aqueous EO₁₆₆-B₁₀₄ solution. The smaller PEO/PB volume ratio favors the cylindrical geometry. Core-corona structure is again evident at an under-focus of 0.7 μm .

tion that the optical density is proportional to chain concentration density. It is noteworthy that the density falls smoothly at the edge of each micelle, not abruptly as a step in the star and mean density models. Another feature of the micrograph is that the spherical micelles are ordered in a fairly regular hexagonal array. Presumably this ordering is in response to the thickness gradient of the biconcave film which is about 10–20 nm thick in the center (upper part of the Figure 2) and 200–300 nm thick at the edge of the hole (lower part in Figure 2) it spans in the support film. That is, micelles are forced away from the thin central region and segregate toward the thicker edge. They even overlap (in the trajectory of the electron beam) in the thickest part of the perimeter, which results in the seemingly fused corona regions of some of the adjacent micelles in the lower part of Figure 2. Presumably the hexagonal array formed in response to the repulsion between the micelles. The interaction potentials between polymer brushes on spherical interfaces were calculated to be steeply repulsive; those of long-hair micelles are found to be close to hard spheres.¹⁰ Ordered arrays of either body-centered cubic (BCC) or face-centered cubic (FCC) symmetry have been observed to form in polymeric micellar systems at moderate solution concentrations.²² The core diameter and the total micelle diameter including the extended corona determined from the density profile are 15 ± 1 nm and 48 ± 1 nm, respectively. The narrow distribution of the micelle size agrees well with the predictions.²⁸

Similar to surfactant aggregation, reducing the volume ratio of PEO (the “head group”) gives rise to smaller interfacial curvature, driving the transition from the spherical to cylindrical micelles or even lamellar structure (not shown). Figure 3 shows a typical micrograph of the EO₁₆₆-B₁₀₄ solution. The core-corona structure is evident. The core diameter is 16 ± 1 ; the total diameter is 49 ± 1 nm. EO₅₆-B₄₅ also forms wormlike micelles (Figure 4), with a core diameter of 20 ± 1 nm and corona thickness of 13 ± 1 nm. With these data, the theoretically predicted scaling relationship between core and corona dimensions can be tested directly. In Table 2, the experimentally observed core and corona sizes are compared with those predicted by the “mean density model”,¹⁴ viz., $R_{\text{core}} \propto N_{\text{PB}}^{2/3}$,

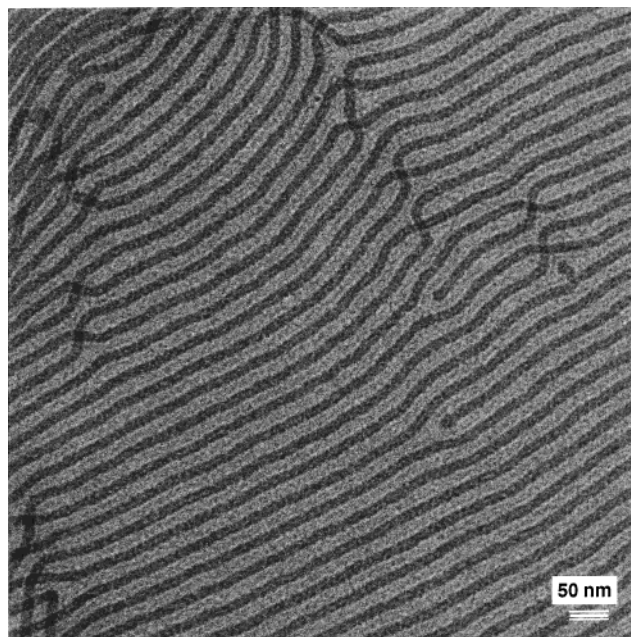


Figure 4. Long cylindrical micelles formed when PEO/PB volume ratio was further reduced to EO₅₆-B₄₅. The alignment of the micelles was presumably in response to the thinness (around 10 nm) of the thin vitreous ice film in which the micelles were suspended.

TABLE 2: Comparison of Core to Total Core-Corona Size Ratios

	experimental values $R_{\text{core}}/R_{\text{total}}$	star model $R_{\text{core}}/R_{\text{total}}$		mean density model $R_{\text{core}}/R_{\text{total}}$
		spherical	cylindrical	
EO ₁₂₆ -B ₄₅	0.31	0.293	0.189	0.123
EO ₁₆₆ -B ₁₀₄	0.32	0.359	0.290	0.146
EO ₅₆ -B ₄₅	0.43	0.477	0.426	0.236

$R_{\text{total}} \propto N_{\text{PB}}^{1/5} N_{\text{EO}}^{4/5}$, and by the “star model” of spherical micelles¹: $R_{\text{core}} \propto N_{\text{PB}}^{3/5}$, $R_{\text{total}} \propto N_{\text{PB}}^{4/25} N_{\text{EO}}^{3/5}$; and of cylindrical micelles: $R_{\text{core}} \propto N_{\text{EO}}^{-1/2} N_{\text{PB}}^{7/6}$, $R_{\text{total}} \propto N_{\text{PB}}^{1/3} N_{\text{EO}}^{1/2}$. The scaling relationship of cylindrical micelles formed by an A-B diblock copolymer can be derived similarly to that of spherical micelles by employing corresponding expressions of free energy contributions (core, corona, and interface) in cylindrical configurations. The R_{core} and R_{total} probably share the same prefactor, as has been assumed here. However, the prefactors are not known and they probably differ from copolymer to copolymer.

As expected, the star model agrees better with the TEM measurements than the mean density model. That it agrees as well as it does, despite the star model’s assumption that $N_{\text{B}} \ll N_{\text{A}}$, suggests that the scaling relationship from the star model may apply to a broader range of copolymer block size. The predictions of the star model do fall a little short of the experimental values. Among possible reasons are finite molecular weight effects and the scaling models’ assumptions that all chain ends are located at the same height and fluctuations in chain extension can be ignored. End segments extending beyond the average brush height incur a lower energetic penalty than the middle segments, so that the chain ends form a “tail” region in the segment density distribution.²⁹ The tail region can be seen in the density profile measured directly from a TEM micrograph (inset of Figure 2). Furthermore, the star model takes into account neither the configurational entropy of the PB chains nor the localization of A-B joints at the core interface. To our knowledge, no self-consistent-field (SCF) analysis has predicted

thermodynamic properties of polymeric micelles such as the micellar size and graft density (aggregation number) that can be tested by the Cryo-TEM data. Because the relationships between corona (brushes) thickness and corona chain length predicted by available SCF theories depend on the geometry of the brushes, more specimens of each kind of micelle are necessary for a sound comparison.

The kinetics and equilibration of polymeric micelles is an issue. Concerns about the equilibration of block copolymer micelles have been raised on grounds of the kinetic theory of micellization via stepwise monomer–micelle exchange by Aniansson et al.,³⁰ according to which strongly hydrophobic chains result in a greatly reduced monomer exit rate, i.e., rate of monomers leaving a micelle, and therefore extremely slow approach to equilibrium. However, a micellar system can equilibrate by another route, namely the “fission and growth process”,³¹ by which large micelles divide into smaller ones, then grow by adding monomers, thus avoiding the restraint of the low monomer exit rate and reaching equilibrium much more readily. The PEO–PB copolymer in the presented work was dissolved directly into water, no precursor solvent was used. Accordingly, we believe the micelles that were imaged had reached thermal equilibrium via the relatively rapid fission processes. In our experiments, rate of equilibration appears not to be a problem because images of a sample made 1 day after it was prepared did not differ any discernibly in micellar shape or size from those stored for a month.

Block copolymers are in many aspects the macromolecular counterparts of ordinary, low molecular weight surfactants. Yet, these polymeric “surfactants” exhibit features that have no direct analogues among surfactants, notably aggregate/solvent interactions and or inter-aggregate interactions. These features can be largely attributed to the presence of the corona region in the self-assembled polymer microstructures rather than the comparatively sharp boundary of the self-assembled surfactant aggregates. That the corona region can now be visualized directly is the result of advances in the Cryo-TEM technique, viz., better optics (hence better image contrast), digital imaging, and mounting experience with both. This high-resolution direct imaging technique is applicable, we believe, to block copolymers not only in aqueous systems but also in organic solvents, which have already been imaged at lower resolution.³²

Acknowledgment. This work was supported in part by the Center for Interfacial Engineering (CIE), the Materials Research

Science and Engineering Center (MRSEC) at the University of Minnesota, and a grant from the United States–Israel Binational Science Foundation (BSF), Jerusalem (to H.T.D., L.E.S., and Y.T.). We thank T. P. Lodge for helpful discussions.

References and Notes

- (1) Halperin, A. *Macromolecules* **1987**, *20*, 2943–2946.
- (2) Milner, S. T. *Science* **1991**, *251*, 905–914.
- (3) Halperin, A.; Tirrell, M.; Lodge, T. P. *Adv. Polym. Sci.* **1992**, *100*, 31–71.
- (4) Alexander, S. J. *Phys. (Paris)* **1976**, *38*, 977.
- (5) de Gennes, P. G. *Macromolecules* **1980**, *13*, 1069–1075.
- (6) Murat, M.; Grest, G. S. *Macromolecules* **1991**, *24*, 704.
- (7) Milner, S. T.; Witten, T. A.; Cates, M. E. *Macromolecules* **1988**, *21*, 2610–2619.
- (8) Dan, N.; Tirrell, M. *Macromolecules* **1992**, *25*, 2890–2895.
- (9) Wijmans, C. M.; Scheutjens, J. M. H. M.; Zhulina, E. B. *Macromolecules* **1992**, *25*, 2657–2665.
- (10) Lin, E. K.; Gast, A. P. *Macromolecules* **1996**, *29*, 390–397.
- (11) Birshstein, T. M.; Zhulina, E. B.; Khokhlov, A. R.; Yurasova, T. A. *Polym. Sci. U.S.S.R.* **1987**, *29*, 1293.
- (12) Daoud, M.; Cotton, J. P. *J. Physique* **1982**, *43*, 531–538.
- (13) Cosgrove, T.; Heath, T.; Van Lent, B.; Leemakers, F.; Scheutjens, J. *Macromolecules* **1987**, *20*, 1692.
- (14) Leibler, L.; Orland, H.; Wheeler, J. C. *J. Chem. Phys.* **1983**, *79*, 3550.
- (15) Mir, Y.; Auroy, P.; Auvray, L. *Phys. Rev. Lett.* **1995**, *75*, 2863–2866.
- (16) Auroy, P.; Auvray, L.; Léger, L. *Phys. Rev. Lett.* **1991**, *66*, 719–722.
- (17) Penfold, J. e. a. *J. Chem. Soc., Faraday Trans.* **1997**, *93*, 3899–3917.
- (18) Perahia, D. G. e. a. *Phys. Rev. Lett.* **1994**, *72*, 100–103.
- (19) Xu, R.; Winnik, M. A.; Riess, G.; Chu, B.; Croucher, M. D. *Macromolecules* **1992**, *25*, 644–652.
- (20) Nolan, S. L.; Phillips, R. J.; Cotts, P. M.; Dungan, S. R. *J. Colloid Interface Sci.* **1997**, *191*, 291–302.
- (21) Zhang, L.; Barlow, R. J.; Eisenberg, A. *Macromolecules* **1995**, *28*, 6055–6066.
- (22) McConnell, G. A.; Gast, A. P.; Huang, J. S.; Smith, S. D. *Phys. Rev. Lett.* **1993**, *71*, 2102–2105.
- (23) Amiel, C. e. a. *Macromolecules* **1995**, *28*, 3125–3134.
- (24) Struis, W. J.; Eicke, H. F. *J. Phys. Chem.* **1991**, *95*, 5989–5996.
- (25) Talmon, Y. *Ber. Bunsen-Ges. Phys. Chem.* **1996**, *100*, 364.
- (26) Mortensen, K.; Talmon, Y.; Gao, B.; Kops, J. *Macromolecules* **1997**, *30*, 6764–6770.
- (27) Won, Y.-Y.; Davis, H. T.; Bates, F. S. *Science* **1999**, *283*, 960–963.
- (28) Johner, A.; Joanny, J. F. *Macromolecules* **1990**, *23*, 5299–5311.
- (29) Witten, T. A.; Leibler, L.; Pincus, P. A. *Macromolecules* **1990**, *23*, 824.
- (30) Aniansson, E. A. G. e. a. *J. Phys. Chem.* **1976**, *80*, 905–922.
- (31) Kahlweit, M. J. *Colloid Interface Sci.* **1982**, *90*, 92.
- (32) Oostergetel, G. T.; Esselink, F. J.; Hadziioannou, G. *Langmuir* **1995**, *11*, 3721.